ACS OMEGA

Open Access

http://pubs.acs.org/journal/acsodf

Article

Study on Matrix Damage and Control Methods of Fracturing Fluid on Tight Sandstone Gas Reservoirs

Xueping Zhang,* Youquan Liu, Lang Zhou, Chuanrong Zhong, and Pengfei Zhang

Cite This: *ACS Omega* 2023, 8, 37461−37470

Read Online

ACCESS | Metrics & More | Article Recommendations

ABSTRACT: Hydraulic fracturing is a highly effective method for stimulating the development of gas reservoirs. However, the process of pumping fracturing fluid (FF) into the reservoir unavoidably causes damage to the surrounding matrix, leading to a decrease in the overall stimulation effect. To assess the extent of matrix permeability damage caused by the intrusion of FF, as well as its impact on the pore throat structure, and to propose appropriate measures to control this damage, we conducted a series of experimental studies on tight gas reservoirs. These studies included mercury intrusion, core flow, nitrogen adsorption, linear expansion, and contact angle measurements. The findings revealed that the damage inflicted on matrix permeability by FF was significantly greater than that caused by its gel-breaking counterpart. Surprisingly, the damage rate of the rejecting fluid to the matrix was found to be comparable to that of its gel-breaking counterpart. The fractal dimension (D_2) was observed to have a strong correlation with surface area, pore volume, and mean pore size, making it an effective means of characterizing pore structure characteristics. After the rock samples were displaced by the formation water, the D_2 value decreased, leading to a decrease in the complexity of the pore throat structure and an increase in matrix permeability. Conversely, the displacement of the FF increased the D_2 value, indicating a gradual complication of the pore throat structure and a more uneven distribution of pore sizes. The inclusion of polyamide in antiexpansion FF, as well as its gel-breaking counterpart, proved to be effective in inhibiting the hydration and expansion of clay minerals, thereby reducing water-sensitive damage. Additionally, the use of surfactants with low surface tension enhanced the flowback rate of FF by increasing the contact angle and reducing the work of adhesion. This, in turn, helped to decrease the apparent water film thickness and expand gas flow channels, ultimately improving gas permeability.

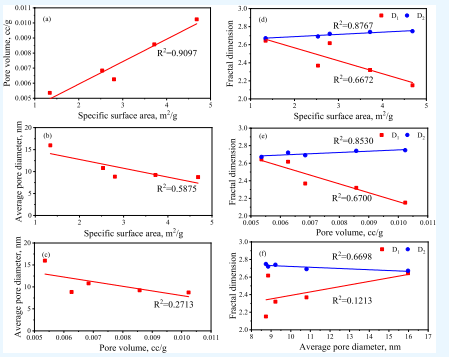

1. INTRODUCTION

In the past few years, there has been rapid growth in the exploration and development of unconventional oil and gas resources, specifically tight oil and gas. Hydraulic fracturing technology has emerged as an essential method for constructing the capacity necessary to extract these types of resources. It achieves the effective transformation of reservoirs by creating a complex network of fractures.[1−3] However, when compared to other regions, the Jurassic Shaximiao Formation of the Qiulin Block in the central Sichuan Basin holds shallowly buried and easily constructed wells,[4] natural fractures within reservoirs are not well-developed. Consequently, it becomes challenging to establish a complex fracture network through hydraulic fracturing alone. The current volumetric fracturing technology used in modifying the tight sandstone gas reservoir in this region has shown significant incompatibility. Therefore, there is a need to enhance the volumetric fracturing technology to realize the advantageous development of tight sandstone gas.

The Shaximiao Formation's tight gas reservoir in the Qiulin Block of the Sichuan Basin exhibits distinct characteristics, including a dense matrix, underdeveloped natural fractures, small pore throat radius, limited pore connectivity, and abundant clay minerals. Consequently, it has a high potential for reservoir damage.[5,6] The primary spaces and channels responsible for fluid flow in the sandstone reservoir of the Shaximiao Formation in the Qiu Lin Block are the pores and throats with a median radius ranging from 0.128 to 0.599 μm. The small size of these pores and throats increases the susceptibility of the reservoir to secondary damage caused by the fracturing fluids (FFs). Extensive research has demonstrated that physical and chemical damage are the primary types of damage in tight reservoirs, which can be attributed to various mechanisms including fluid sensitivity, intrusion by solid particles, phase trapping, sensitivity to stress, and adsorption of treatment agents.[7−9]

Received: July 31, 2023
Accepted: September 12, 2023
Published: September 27, 2023

https://doi.org/10.1021/acsomega.3c05461
ACS Omega 2023, 8, 37461−37470

Table 1. Mineral Content (wt %) of the Sandstone Samples Determined by XRD

mass fraction of mineral						mass fraction of clay mineral			
quartz	orthoclase	plagioclase	calcite	pyrite	clay	illite/smectite	illite	kaolinite	chlorite
40.3	6.2	34.7	1.7	0.4	16.7	31	39	25	5

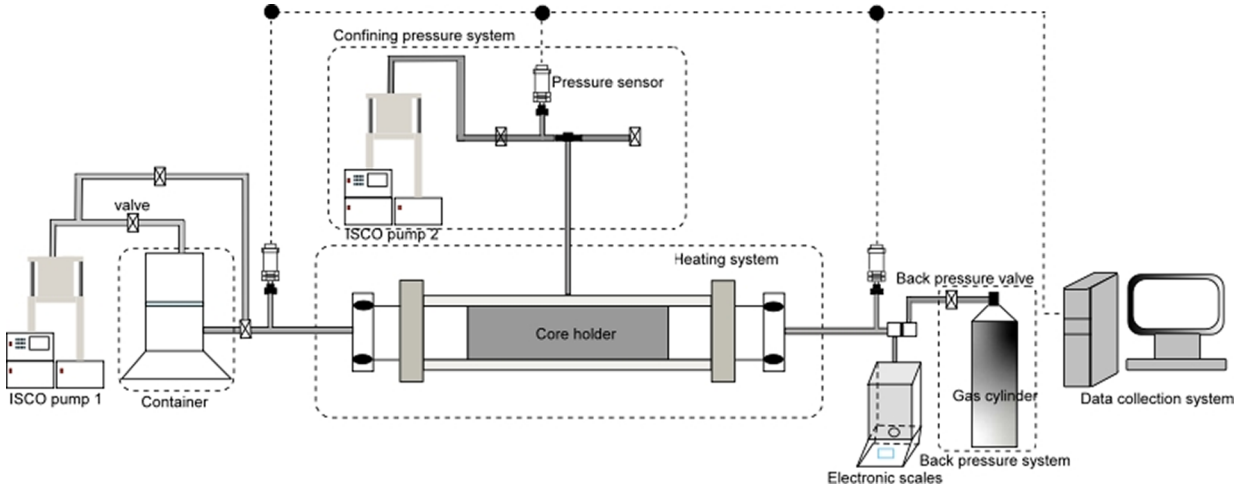

Figure 1. Schematic diagram of core displacement experimental equipment.

Tight sandstone reservoirs are characterized by low permeability, low porosity, and strong capillary forces, making them prone to permeability damage resulting from the invasion of foreign fluids during reservoir development.[10−14] The interaction between foreign fluids and the formation can lead to hydration, swelling, dispersion, and migration of clay minerals, ultimately causing a reduction in formation permeability. FFs, such as the fluids used to fracture and modify oil and gas formations, serve the purpose of transferring pressure and carrying proppants during the fracturing process. However, they also pose a significant risk of damaging the reservoir, thereby causing varying degrees of harm.[15,16]

Currently, the assessment of water sensitivity in tight reservoirs primarily relies on core flow experiments. These experiments allow for the quantification of the extent and direction of reservoir damage due to sensitivity. To gain further insight into the damage mechanisms, various core analysis tools such as cast thin section observation, XRD diffraction analysis, scanning electron microscopy, and micro and nano CT techniques are employed.[17−20] Numerous researchers have investigated formation sensitivity using conventional core flow experiments in combination with microcore analysis techniques like CT and nuclear magnetic resonance (NMR). One study utilized X-ray microcomputed tomography (CT) analysis to evaluate formation damage in sandstone reservoirs, providing conclusive evidence of damage caused by clay swelling and fine migration during workover fluid and formation fluid flooding.[21] To address water sensitivity damage in tight reservoirs, the addition of clay stabilizers to FF formulations has proven effective. Consequently, a considerable number of clay stabilizers with antiexpansion properties have been developed and continuously optimized.[22]

The enhanced understanding of water-lock damage in tight reservoirs primarily came from quantitative assessment and investigation of its mechanisms, utilizing displacement nuclear magnetism and imbibition flowback evaluation. Core flow and NMR techniques were used to explain the mechanism of formation damage caused by FF imbibition during operations, such as fracturing, well shut-in, and rejection. This understanding revealed that formation damage was more severe in sandstone cores with low permeability due to the strong retention of FF.[23] The accumulation of water in the formation resulted in significant damage to water-phase traps, which negatively impacted gas production in tight reservoirs.[24] To improve gas well productivity in such reservoirs, it is crucial to implement effective damage control measures.[25] Current strategies focus on reducing adhesion work, water saturation, and the apparent thickness of water films to mitigate water-phase trapping damage and restore rock permeability.[26] Surfactants with low surface tension are widely acknowledged for their indispensable role in enhancing the rejection rate of FFs and minimizing water-phase trap damage.[27] Fluorocarbon and amphoteric surfactants and wetting reversal agent were compounded and developed as water unlocking agents suitable for gas well production enhancement.[28,29]

In this study, we investigated the damage caused to matrix permeability by the displacement of various FFs in the tight sandstone of the Shaximiao Formation in the Qiulin Block of the Sichuan Basin. We also employed low-temperature nitrogen adsorption experiments and the fractal dimension method to uncover the impact of different fluid displacements on the pore throat of tight sandstone. Furthermore, we analyzed the control methods for mitigating the damage to tight sandstone reservoirs caused by FFs.

2. MATERIALS AND METHODS

2.1. Material. Tight gas reservoir cores from the Shaximiao Formation in the middle Sichuan Basin were collected in the field for experimental purposes. Various fluids, such as distilled water (DI), simulated formation water, FF, gel-breaking fracturing fluid (GFF), rejection fluid (RF) and gel-breaking rejecting fluid (GRF) were utilized during the experiments. The combinations and additives of the displacement fluids in this work are as follows:

https://doi.org/10.1021/acsomega.3c05461
ACS Omega 2023, 8, 37461−37470

Table 2. Pore Structure of Samples by Mercury Intrusion Porosimetry

core no.	porosity, %	permeability, mD	median pore throat radius, μm	maximum mercury saturation, %	residual mercury saturation, %
S1	8.03	0.0475	0.1094	90.12	66.14
S2	9.21	0.0682	0.3506	92.21	68.73

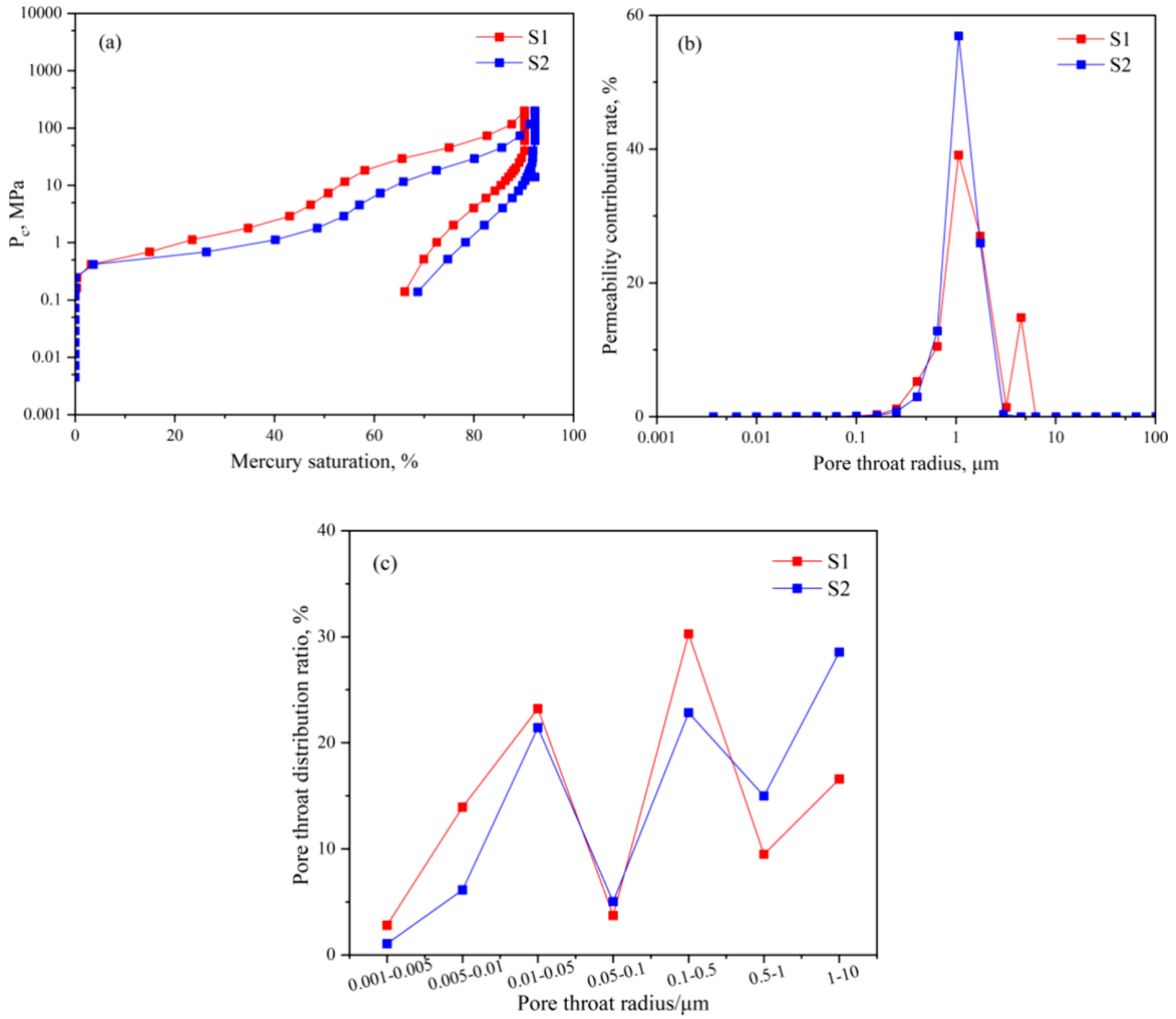

Figure 2. Capillary pressure analysis by mercury pressure method: (a) capillary curve; (b) permeability contribution; and (c) pore throat distribution

SWF: DI + 2.0% KCl + 5.5% NaCl + 0.45% $MgCl_2$ + 0.55% $CaCl_2$;

FF: DI + friction reducer + 0.1% cationic cleanup additive + 0.05% emulsion breaker;

GFF: DI + friction reducer + 0.1% cationic cleanup additive + 0.05% emulsion breaker + 0.1% ammonium persulfate;

RF: rejection fluid (2276 mg/L Na^+ + 17.2 mg/L K^+ + 10.4 mg/L Mg^{2+} + 1082 mg/L Ca^{2+} + 15.14 mg/L Fe^{3+} + 2978 mg/L Cl^- + 12.53 mg/L SO_4^{2-} + 8.26 mg/L CO_3^{2-}) + friction reducer + 0.1% cationic cleanup additive + 0.05% emulsion breaker;

GRF: rejection fluid+friction reducer + 0.1% cationic cleanup additive + 0.05% emulsion breaker + 0.1% ammonium persulfate;

To determine the composition of the entire rock and clay minerals, an XPert3Powder model X-ray diffractometer was used. The clay mineral content, which amounted to 16.7%, is specified in Table 1. For evaluating the pore throat distribution of the sandstone sample, the Autopore IV 9520 mercury intrusion meter provided by Micromeritics (Shanghai) Instruments Co. was employed. Furthermore, nitrogen adsorption measurements at low temperatures were conducted using the ASAP 2020 plus HD88 fully automatic gas adsorption device also supplied by Micromeritics (Shanghai) Instruments Co.

2.2. Method. *2.2.1. Permeability Damage Evaluation.* After the core sample was chosen, its diameter and length were measured and documented by using vernier calipers. The core was then displaced by compound formation water using a versatile core displacement device (Figure 1) to determine its initial permeability, referred to as K_1, which represents the permeability before any damage occurred. To assess the impact of damage, the core was displaced by using a compound FF,

https://doi.org/10.1021/acsomega.3c05461
ACS Omega 2023, 8, 37461−37470

Table 3. Core Parameters and Results of Permeability Damage[a]

core no.	length, cm	diameter, cm	porosity, %	permeability, mD	invading fluid	damage rate, %	damage degree
1	5.01	2.50	8.03	0.0290	0.1% FF	51.72	moderate to strong
2	5.02	2.51	9.21	0.0380	0.1% RF	57.43	moderate to strong
3	5.01	2.51	9.34	0.0386	0.1%GFF	20.49	weak
4	5.00	2.50	9.02	0.0300	0.1%GRF	50.34	moderate to strong
5	5.01	2.52	9.56	0.0556	0.4%FF	58.98	moderate to strong
6	5.02	2.51	9.64	0.0424	0.4%RF	60.86	moderate to strong
7	5.01	2.50	9.42	0.0491	0.4%GFF	27.14	weak
8	5.00	2.50	10.02	0.0619	0.4%GRF	64.56	moderate to strong
9	5.02	2.51	9.86	0.0522	1%FF	72.68	strong
10	5.01	2.50	8.95	0.0752	1%RF	67.05	moderate to strong
11	5.01	2.50	8.04	0.0266	1%GFF	40.44	moderate to weak
12	5.00	2.51	10.26	0.0691	1%GRF	76.19	strong

[a]Notation: FF, RF, GFF, and GRF represent FF, rejecting fluid, gel-breaking FF, and gel-breaking rejecting fluid, respectively.

allowing for the determination of the core permeability at the time of damage. Subsequently, the core was displaced using compound formation water to determine the core permeability after damage, denoted as K_2. The rate of permeability damage was calculated by using eq 1. The evaluation of the extent of damage caused by the FF on tight sandstone was conducted based on the assessment criteria for FF damage to reservoirs.[30]

$$\eta_d = \frac{K_1 - K_2}{K_1} \quad (1)$$

where η_d represents permeability damage rate, %; permeability of the matrix before the core is squeezed into the FF, mD; K_1 and K_2 denote the permeability of cores before and after damage by squeezing in FF, mD, respectively.

2.2.2. Low Temperature Nitrogen Adsorption Measurement. The rock samples at the beginning, as well as those affected by various fluids, were crushed and dried to eliminate any moisture on the surface. To analyze their specific surface properties, nitrogen adsorption and desorption tests were conducted by using a Micromeritics ASAP 2020 plus HD88 specific surface analyzer. By examining the correlation between the pressure at 77.46 K and the adsorption volume of N_2, we obtained information about the pore volume, specific surface area, and distribution of pore sizes in the sandstone samples.

2.2.3. Linear Expansion Experiment. The linear expansion rate of dense sandstone was assessed using the OFI150-80-1 dynamic linear expansion apparatus to select the most suitable antiexpansion agent. 10 g of dried core powder, which was precisely weighed and sieved to 100 mesh size, was compacted into small cylindrical rock samples under a pressure of 20 MPa. The resulting samples were then placed in the apparatus, and the linear expansion rate along the axial direction was promptly measured after the working fluid was mixed.

2.2.4. Contact Angle Measurement. The Kruss-DSA100 contact angle measuring instrument was utilized to measure the contact angle on the initial rock sample as well as on the rock sample after being affected by the FF and breaking fluid. A prepared rock slice was subjected to water droplets, and the extent of their spreading on the surface was recorded. Software analysis was employed to evaluate the contact angle and interface tension with the measurements being repeated three times for an average value.

Spontaneous diffusion and wetting processes of liquids on solid surfaces occur naturally. The work of adhesion represents the energy required to overcome the intermolecular forces between the two phases and separate the interface between the liquid and solid phases. This concept can be expressed in eq 2:

$$W_a = \gamma_{SG} + \gamma_{LG} - \gamma_{SL} = \gamma_{LG}(1 + \cos\theta) \quad (2)$$

where W_a is the work of adhesion between the solid−liquid interface in air, mN/m; θ is the contact angle, degree; and γ_{SG}, γ_{LG}, and γ_{SL} denote gas−solid, liquid−solid, and gas−liquid interface tensions, respectively.

3. RESULTS AND DISCUSSIONS

3.1. Matrix Permeability Damage of FF to Tight Sandstone. The rock samples were analyzed to determine their pore throat properties using a mercury intrusion measurement. The findings are presented in Table 2. Additionally, the capillary analysis of the rock samples was conducted using the mercury-pressure method, and the results are depicted in Figure 2. The median pore throat radii for the two rock samples were determined to be 0.1094 and 0.3506, respectively. The majority of the pore throat radii fell within the range of 0.1−0.5 μm. The pore throat radius distribution that primarily influenced the core permeability of the rock samples spanned 0.1−10 μm. The peak pore throat radius contributing to permeability was approximately 1 μm, indicating that the rock sample's permeability is mainly governed by the presence of larger pores.

The experiment involved selecting tight sandstone rock samples that had gas-measured permeability ranging from 0.01 to 0.1 mD and porosity between 8 and 10.3%. The purpose was to conduct matrix permeability damage experiments while eliminating the influence of pore permeability properties on the test results. To simulate the impact of various FFs on reservoir damage, different fluids were chosen for the core damage experiments: FF, gel-breaking fluid, RF, and gel-breaking RF. The concentrations of the drag-reducing agent in the different fluids were set at 0.1, 0.4, and 1% to assess the level of damage to reservoir permeability during fracturing operations. The residue contents of 0.1, 0.4, and 1% FFs after breaking in fresh water were determined to be 86, 226, and 488 mg/L, respectively. However, the residue content after breaking of 0.1, 0.4, and 1% FF formulated with RF was significantly higher than that in fresh water, which was evaluated as 265, 950, and 2015 mg/L, respectively. The core parameters and results of permeability damage are provided in Table 3, while Figure 3 presents a comparison of the matrix damage caused by different fluids in tight sandstone. The findings indicate that the FF induces greater damage to

https://doi.org/10.1021/acsomega.3c05461
ACS Omega 2023, 8, 37461−37470

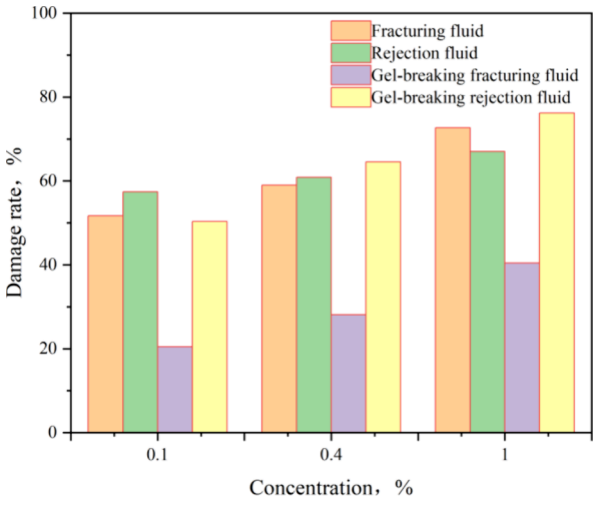

Figure 3. Comparison of the matric damage degree of different fluid to tight sandstone.

the matrix permeability compared to its gel-breaking counterpart and that the overall degree of permeability damage progressively increases with higher concentrations of the resistance reducer. The permeability damage rate of the RF at 0.4 and 1% resistance reducer loading is lower than that in its broken state, whereas at 0.1% addition, it is higher. This difference is primarily due to the presence of a high residue content in the gel-breaking RF under a high-resistance reducer loading. The abundant residue blocks the gas seepage channels, leading to significant solid phase damage, which predominantly contributes to the total damage. The damage caused by the gel-breaking RF is consistently higher than that caused by the fracturing gel-breaking fluid. This discrepancy can be attributed to pore throat blockage resulting from the interaction between high-valent metal salt ions in the RF and the polymer, leading to flocculation precipitates. The viscosity of the FF prepared with the RF decreases significantly compared to that prepared with water under the same resistance reducer loading. This decrease in viscosity-induced liquid-phase retention damage is accompanied by a notable increase in residue-induced solid phase damage. Ultimately, the disparity in matrix damage between the FF and the RF is not significant. However, the damage is notably more severe in the gel-breaking RF than in the fracturing breaking fluid.

3.2. Effect of Fluid on Reservoir Pore Structure. We examined how the characteristics of tiny pore openings in tight sandstone change when different fluids infiltrate them. We used low-temperature nitrogen adsorption and recorded the findings in Table 4. The specific surface area, volume of tiny pores, and average diameter of these pores in the sandstone samples were altered when various fluids replaced them. When formation water compressed the tight sandstone sample, its specific surface area decreased, but surprisingly, the average pore size increased significantly. However, when the rock sample previously compressed by formation water was replaced with FFs of 0.1 and 0.4% concentrations, there was a gradual rise in specific surface area, accompanied by a corresponding decrease in average pore size. This phenomenon is illustrated by the low-temperature nitrogen adsorption−desorption curves in Figure 4 and the associated pore throat distribution

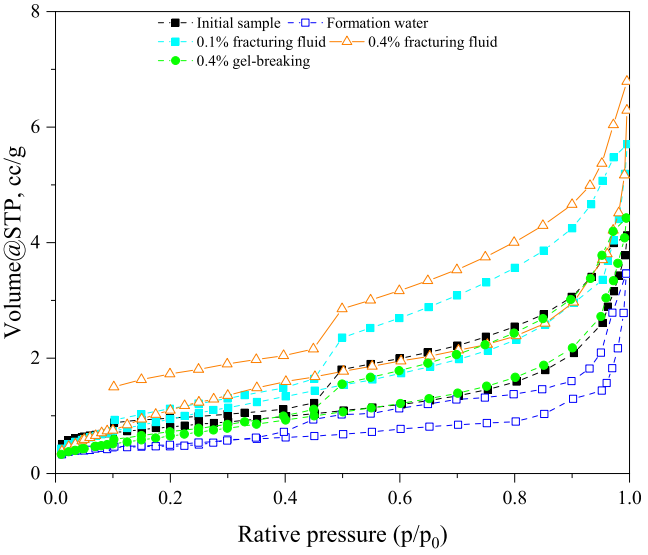

Figure 4. Low-temperature nitrogen adsorption−desorption curves of tight sandstone.

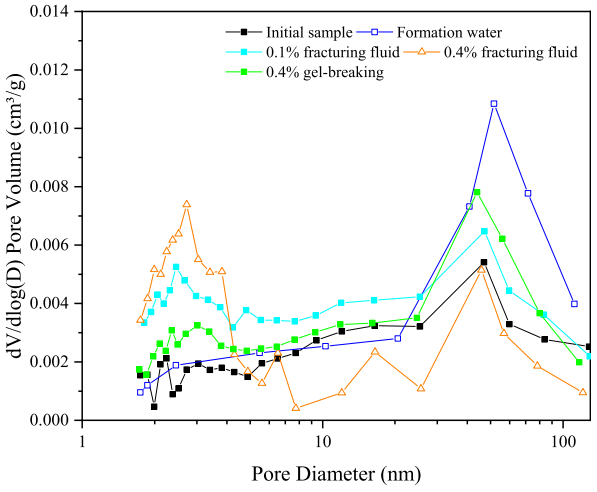

Figure 5. Pore throat distribution of tight sandstone.

as shown in Figure 5. The figure demonstrates that the flow of fluids through porous materials is primarily influenced by

Table 4. Pore Structure of Sample Treated by Different Fluid

treatment agents	specific surface area, m^2/g	pore volume, cc/g	average pore diameter/nm
untreated	2.8034	0.006261	8.8478
formation water	1.3410	0.005356	15.9757
0.1% fracturing fluid	3.7202	0.008575	9.2195
0.4% fracturing fluid	4.6860	0.010238	8.7389
0.4% gel-breaking fluid	2.5337	0.006842	10.8018

https://doi.org/10.1021/acsomega.3c05461
ACS Omega 2023, 8, 37461−37470

Table 5. Fractal Dimension of Tight Sandstone Derived from the Fractal FHH Model

sample	$p/p_0 < 0.5$			$p/p_0 > 0.5$		
	fitting equation	R^2	D_1	fitting equation	R^2	D_2
initial sample	$y = -0.3831x - 0.0364$	0.9926	2.6169	$y = -0.2795x + 0.0360$	0.9696	2.7205
formation water	$y = -0.3560x - 0.5219$	0.9679	2.6440	$y = -0.3289x - 0.5278$	0.9891	2.6711
0.1% fracturing fluid	$y = -0.6803x + 0.2408$	0.9949	2.3197	$y = -0.2590x + 0.4124$	0.9820	2.7410
0.4% fracturing fluid	$y = -0.8487x + 0.4192$	0.9779	2.1513	$y = -0.2516x + 0.4990$	0.9958	2.7484
0.4% gel-breaking	$y = -0.6316x - 0.1355$	0.9991	2.3684	$y = -0.3089x - 0.0236$	0.9778	2.6911

viscosity. Highly viscous FFs tend to remain trapped in the rock pores, reducing the available flow paths, while formation water expands the flow paths, thereby improving the permeability of the matrix.

The method of low-temperature nitrogen adsorption is appropriate for assessing the pores in compact sandstone with pore sizes ranging from 2 to 200 nm. The branch of adsorption in the nitrogen adsorption−desorption curve enables the determination of the distribution of pore sizes and is mostly unaffected by the tensile strength.[31] By examination of the adsorption branch, the pore size distribution and fractal dimension in tight sandstone can be calculated. The calculation of the fractal dimension, using the FHH model,[32] can be represented by eq 3. In this equation, the $\ln(V)$ varies in a linear manner with the $\ln(\ln(P_0/P))$, and the slope is utilized to denote the fractal dimension D.

$$\ln V = (D - 3)\ln\left[\ln\left(\frac{P_0}{P}\right)\right] + C \tag{3}$$

where V is the amount of nitrogen adsorbed at equilibrium pressure P, m^3/g; P_0 is the saturation pressure, MPa; and D is the fractal dimension; C is a constant.

The nitrogen adsorption data of the samples were processed, and the linear equation of the fitted adsorption curves for $\ln(V)$ versus $\ln[\ln(P_0/P)]$ is listed in Table 5. Figure 6 displays

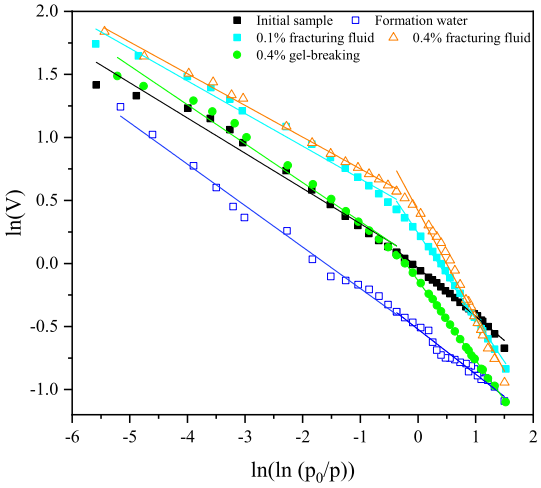

Figure 6. Fractal characteristics of samples based on nitrogen adsorption data.

the fractal characteristic curves of the samples treated with different fluids, based on the nitrogen adsorption data. The fractal dimensions in the low-pressure region ($0 < P/P_0 < 0.5$) and the high-pressure region ($0.5 < P/P_0 < 1$) were investigated by dividing the curve into two segments with the relative pressure of 0.5 as the boundary to characterize the dual fractal dimensions of the pore sizes of less than 2 nm versus those of greater than 2 nm after different fluid treatments. The fractal dimension denoted as D_1 represents the characteristics of the pore surface and is associated with the low-pressure region (pore size $d < 2$ nm). A higher value of D_1 indicates a more irregular and less smooth internal surface of the pore. On the other hand, the fractal dimension denoted as D_2 reflects the characteristics of the pore structure, including the distribution and size of pores, in the high-pressure region (pore size > 2 nm). A larger D_2 value suggests a more dispersed pore size distribution and a smaller pore size. After different fluid treatments, the tight sandstone sample exhibited a larger D_2 value compared to D_1, indicating that the larger pores ($d > 2$ nm) are more complex than the smaller pores ($d < 2$ nm). This implies that the internal pore structure exhibits greater complexity than the pore surface. When rock samples are subjected to various fluids, the fractal dimension D_1 is more influenced by the fluid compared to D_2. This suggests that the fluid primarily affects the roughness of the internal surface of the pore. The introduction of formation water to the rock sample reduces the D_2 value, thereby effectively decreasing the complexity of the pore throat structure and increasing the matrix permeability of the rock sample. However, when the rock sample is treated with FF, the D_2 value gradually increases, indicating that the pore throat of the rock sample becomes more complex and the unevenness of the pore size distribution is enhanced. The extrusion of formation water into the core weakens the smoothness of the pore surface, while the extrusion of FF or gel-breaking fluid enhances it. Scanning electron micrographs in Figure 7 depict the initial rock sample

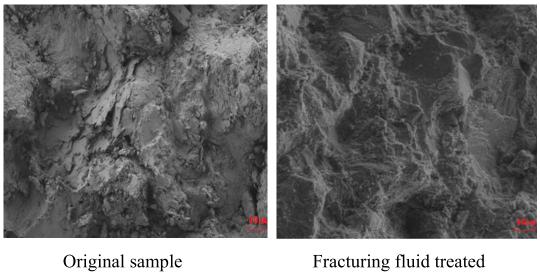

Figure 7. SEM photograph of tight sandstone.

and the sample treated with the FF. The initial sample exhibits tightness with attached tiny particles, poor connectivity between pore throats, and underdeveloped fractures. Following the treatment with FF, a white film is observed on the sample's surface, enhancing its smoothness and increasing the complexity of the pore throat.

The relationship among specific surface area, pore volume, and average pore diameter was examined using linear regression analysis. The results indicated that there is a significant positive correlation between specific surface area

https://doi.org/10.1021/acsomega.3c05461
ACS Omega 2023, 8, 37461−37470

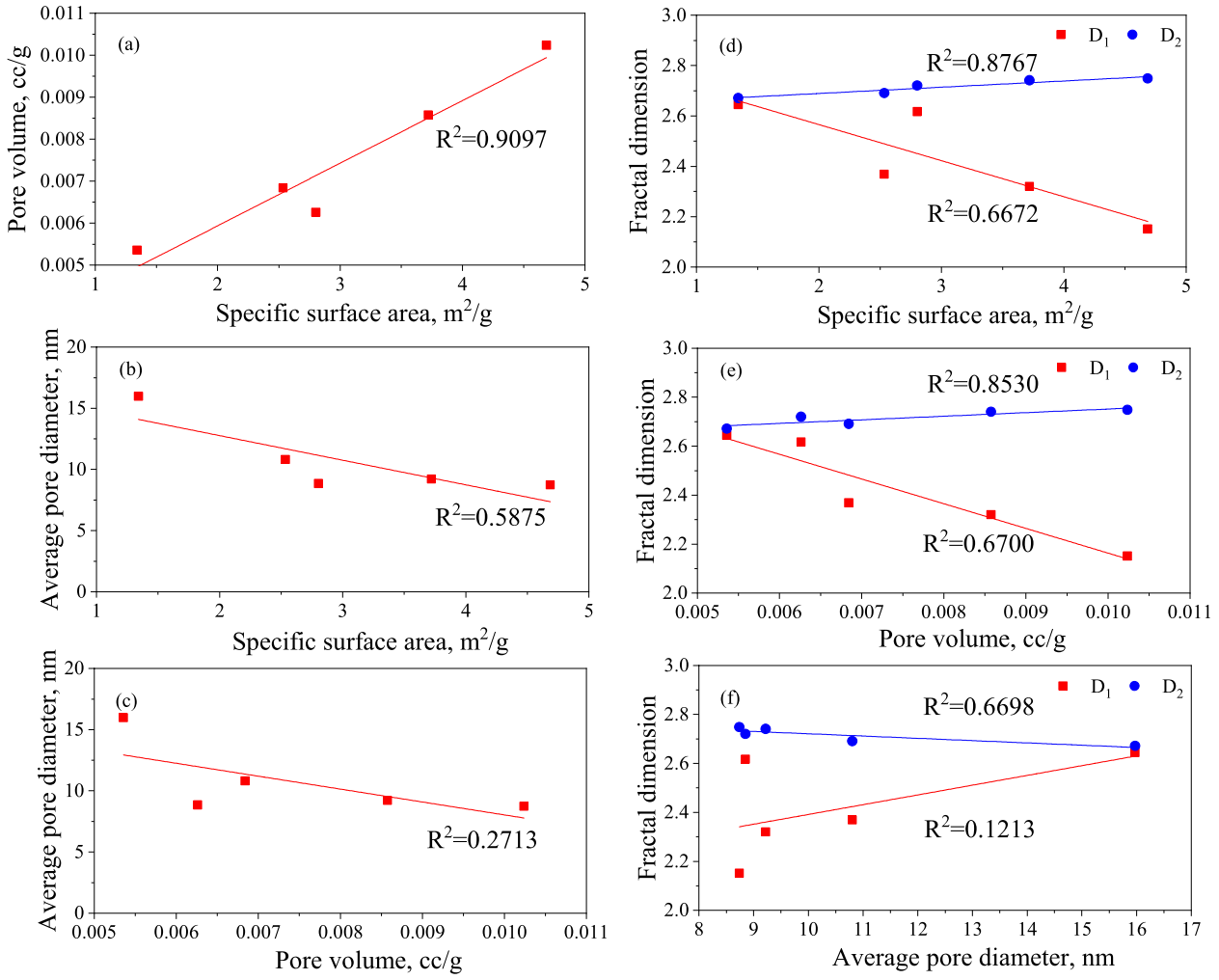

Figure 8. Relationship between fractal dimension and pore structure parameters of tight sandstone samples: (a) pore volume versus specific surface area, (b) average pore diameter versus specific surface area, (c) average pore diameter versus pore volume, (d) fractal dimension versus specific surface area, (e) fractal dimension versus pore volume, and (f) fractal dimension versus average pore diameter.

and pore volume, while average pore diameter has a weak negative correlation with both parameters (Figure 8a–c). This suggests that as the pore size decreases, the pore space and specific surface area within the tight sandstone increase. The fractal dimensions D_1 and D_2 were used in linear regression to model each pore structure parameter. It was observed that D_2 is positively correlated with specific surface area and pore volume but negatively correlated with average pore diameter. These correlations were found to have large coefficients (R^2), indicating that D_2 is a suitable characteristic parameter for assessing pore development. In sandstone samples with a high specific surface area and pore volume, the average pore size is smaller, resulting in a more complex pore structure. On the other hand, the correlation between D_1 and specific surface area, pore volume, and average pore diameter is opposite to that of D_2. Although the correlation is weaker compared with D_2, it still provides a basic characterization of pore surface complexity (Figure 8d–f).

3.3. Method to Reduce Matrix Damage. *3.3.1. Inhibit Hydration Swelling of Clay Mineral.* The degree of damage caused by reservoir water sensitivity is determined by assessing the linear expansion rate of the sample. The water sensitivity evaluation index corresponding to the linear expansion rate of tight sandstone can be referred to the Chinese energy industry standard NB/T 14022-2017.[33] The measurement results are displayed in Figure 9. These results indicate that the tight sandstone sample expands by 5.76% when immersed in distilled water, indicating moderately strong water-sensitive

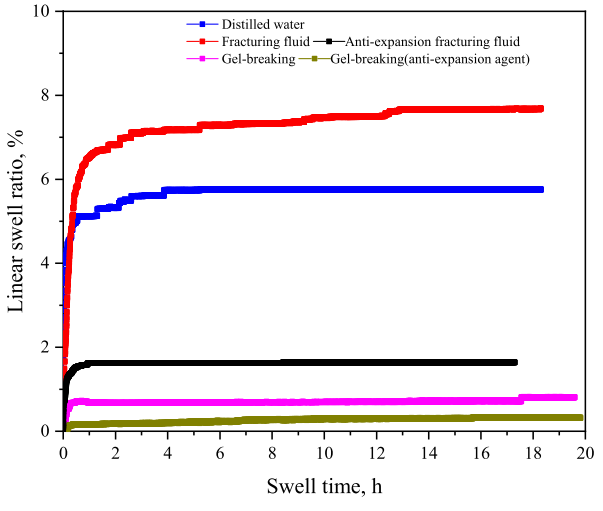

Figure 9. Linear expansion rate results of the tight sandstone samples.

https://doi.org/10.1021/acsomega.3c05461
ACS Omega 2023, 8, 37461−37470

damage. In the FF, the linear expansion rate is 7.69%, indicating strong water sensitivity. However, when exposed to an antiexpansion FF, the linear expansion rate decreases to 1.64%, indicating weak water sensitivity. The linear expansion rates in both the FF and the antiexpansion FF were evaluated as 0.81 and 0.32%, respectively, indicating weak water sensitivity in both cases. The linear expansion rate of the breaking fluid was significantly lower than that of the FF due to the presence of surface-active substances in the breaking fluid that possess antiexpansion properties. The antiswelling rates of the antiswelling FF and the breaking fluid were 78.7 and 95.8%, respectively, demonstrating excellent antiswelling effects. This is attributed to the outstanding performance of polyamide, which is loaded into both the FF and the breaking fluid, in inhibiting the hydration expansion of clay minerals. The polyamide clay stabilizer tends to produce ammonium cations, which adsorb to the clay surface and neutralize the electronegativity of the clay. It can also be adsorbed in the clay intergranular layer, reducing the charged nature of the intergranular layer and the surface. At the same time, it reduces the repulsive force through ion exchange and narrows the intergranular spacing, which ultimately inhibits the hydration and expansion of clay minerals.

3.3.2. Reduce Surface Tension. The experiments involved using different fluids, namely, formation water, FF without cleanup additive, FF, and gel-breaking fluid. These fluids had surface tensions of 37.6, 32.0, 25.6, and 21.5 mN/m, respectively. The purpose was to measure the flowback rate and water lock damage rate of the rock samples. The results, depicted in Figure 10, indicated that fluids with lower surface

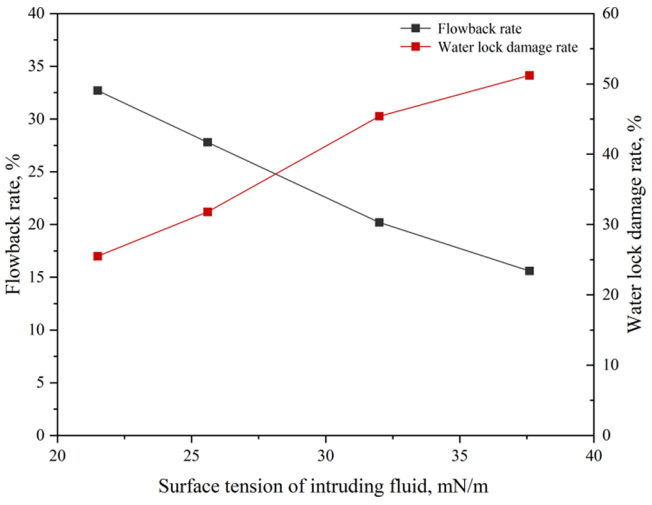

Figure 10. Effect of surface tension of invading fluid on flowback rate and water lock damage rate.

tension were more effective in flowing back from the narrow passages of tight sandstone. This characteristic helped to reduce the water lock damage in low-permeability reservoirs. When compared to the displacement of formation water, the use of low surface tension fluids resulted in a 15.6−32.7% increase in flowback rate and a decrease in water lock damage rate from 51.2 to 25.5%.

Table 6 provides the contact angle, adhesion work, and apparent water film thickness of rock samples treated with different fluids. Figure 11 illustrates the contact angle changes in tight sandstone upon treatment with various fluids. The

Table 6. Contact Angle, Adhesion Work and Apparent Water Film Thickness of Rock Treated by Different Fluid

sample	γ_{LG}, mN/m	contact angle treated by fluid, °	adhesion work treated by fluid, mN/m	apparent water film thickness, nm
untreated	72	34.68	131.21	7.36
fracturing fluid		48.49	119.72	6.35
gel-breaking		57.33	110.87	5.32

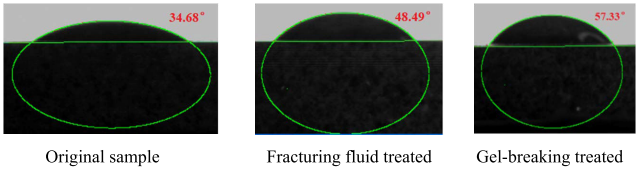

Figure 11. Contact angle of the tight sandstone treated with different fluids.

process for calculating the apparent water film thickness is explained in literature.[34] Initially, the contact angle of the rock samples measures 34.68°. However, after being displaced by low surface tension FF and gel-breaking fluid, the contact angles increase to 48.49° and 57.33°, respectively. A decrease in surface tension of the displacing fluid leads to an increase in contact angle with the rock sample, indicating reduced hydrophilicity and an increased flowback rate. Consequently, the adhesion work and surface water film thickness decrease. Essentially, the surfactant aids in reducing the apparent water film thickness and expanding the gas flow channels, thereby enhancing the gas permeability. The anionic surfactant, while capable of lowering surface tension, will not alleviate water lock damage due to more water wetting the surface. It is concerned that the cleanup additive used is chosen to be a fluorinated cationic surfactant in this work, which effectively reduces surface tension and air-wetted rock surfaces, thus preventing water lock damage damage.[35]

4. CONCLUSIONS

By exploring the characteristics of matrix damage and the effects of different FFs on the pore throat of a tight sandstone reservoir, effective measures to control fluid damage in fracturing operations were proposed. The main conclusions are summarized as follows:

(1) The primary source of matrix damage in tight sandstone reservoirs caused by FF is the liquid phase, as the residue content is low. This damage is controlled by viscosity. The matrix permeability is more affected by the FF compared to its gel-breaking counterpart. Moreover, the degree of overall permeability damage increases with higher loading of resistance reducers.

(2) The fractal dimension D_2 shows a positive correlation with the surface area and pore volume, while it is negatively correlated with the mean pore size, in contrast to D_1. Correlation analysis indicates that D_2 is a better indicator of pore development in tight sandstone reservoirs. The D_2 value decreases after formation water displaces the rock samples, leading to a simpler pore throat structure and increased matrix permeability. FF displacement, on the other hand, increases the D_2 value, suggesting a progressive complexity in the pore throat structure and uneven pore size distribution.

https://doi.org/10.1021/acsomega.3c05461
ACS Omega 2023, 8, 37461−37470

(3) Gel-breaking FF, enriched with surface-active substances, exhibits superior antiexpansion performance compared to antiexpansion FF. The addition of polyamide to antiswelling FF and its gel-breaking variant effectively inhibits clay minerals' hydration and expansion, thereby reducing water-sensitive damage.

(4) We explored the mechanism of mitigating water locking damage in tight sandstone gas reservoirs through the injection of low surface tension FF. Changes in contact angle, adhesion work, and apparent water film thickness were examined. Surfactants with low surface tension enhance the flowback rate of FF by increasing the contact angle and reducing the work of adhesion. This helps reduce the apparent water film thickness and expand gas flow channels, ultimately improving gas permeability.

AUTHOR INFORMATION

Corresponding Author

Xueping Zhang − *Research Institute of Natural Gas Technology, PetroChina Southwest Oil & Gas Field Company, Chengdu, Sichuan 610213, China; College of Energy, Chengdu University of Technology, Chengdu 610059, P. R. China;* orcid.org/0000-0001-7471-6632; Email: zhangxp_1992@sina.com.cn

Authors

Youquan Liu − *Research Institute of Natural Gas Technology, PetroChina Southwest Oil & Gas Field Company, Chengdu, Sichuan 610213, China; Shale Gas Evaluation and Exploitation Key Laboratory of Sichuan Province, Chengdu, Sichuan 610213, China*

Lang Zhou − *Engineering Department, PetroChina Southwest Oil & Gas Field Company, Chengdu, Sichuan 610066, China*

Chuanrong Zhong − *College of Energy, Chengdu University of Technology, Chengdu 610059, P. R. China;* orcid.org/0000-0003-2812-6062

Pengfei Zhang − *Research Institute of Natural Gas Technology, PetroChina Southwest Oil & Gas Field Company, Chengdu, Sichuan 610213, China*

Complete contact information is available at: https://pubs.acs.org/10.1021/acsomega.3c05461

Notes

The authors declare no competing financial interest.

ACKNOWLEDGMENTS

This work is supported financially by the postdoctoral research program of Petrochina Southwest Oil & Gas Field Company (Grant No. 20220302-20).

REFERENCES

(1) Toscano, A.; Bilotti, F.; Asdrubali, F.; Guattari, C.; Evangelisti, L.; Basilicata, C. Recent trends in the world gas market: Economical, geopolitical and environmental aspects. *Sustainability.* **2016**, *8*, 154.

(2) Zhang, Z.; Peng, S.; Ghassemi, A.; Ge, X. Simulation of complex hydraulic fracture generation in reservoir stimulation. *J. Pet. Sci. Eng.* **2016**, *146*, 272−285.

(3) Wang, J.; Zhou, F. J. Cause analysis and solutions of water blocking damage in cracked/non-cracked tight sandstone gas reservoirs. *Petrol Sci.* **2021**, *18*, 219−233.

(4) Xiao, F. S.; Huang, D.; Zhang, B. J.; Tang, D. H.; Ran, Q.; Tang, Q. S.; Yin, H. Geochemical characteristics and geological significance of natural gas in Jurassic Shaximiao Formation. *Sichuan Basin. Acta Petrolei Sinica* **2019**, *40*, 568−576.

(5) Zhang, X. P.; Liu, Y. Q.; Liu, Y. Z.; Zhong, C. R. Influencing factors and application of spontaneous imbibition of fracturing fluids in tight sandstone gas reservoir. *ACS omega.* **2022**, *7*, 38912−38922.

(6) Zhang, X. P.; Liu, Y. Q.; Liu, Y. Z.; Zhong, C. R.; Zhang, P. F. Salt ion diffusion behavior and adsorption characteristics of fracturing fluid in tight sandstone gas reservoir. *Energies.* **2023**, *16*, 2877.

(7) Elkewidy, T. I. Evaluation of formation damage /remediation potential of tight reservoirs. *SPE European Formation Damage Conference & Exhibition.* SPE, The Netherlands, 2013.

(8) Qutob, H.; Byrne, M.; Senergy, L. R. Formation damage in tight gas reservoirs. *SPE European Formation Damage Conference and Exhibition.* SPE, Hungary, 2015.

(9) Saboorian-Jooybari, H.; Pourafshary, P. Potential severity of phase trapping in petroleum reservoirs: An analytical approach to prediction. *SPE Journal.* **2017**, *22*, 863−874.

(10) Yang, S. L.; Wei, J. Z.; *Fundamentals of Petrophysics*, 2nd ed.; Springer: Berlin, 2017, 239−295.

(11) Civan, F. *Reservoir Formation Damage*, 3rd ed.; Gulf Professional Publishing: Waltham, 2015, 1−25.

(12) Liang, T. B.; Gu, F. Y.; Yao, E. D.; Zhang, L. F.; Yang, K.; Liu, G. H.; Zhou, F. J. Formation damage due to drilling and fracturing fluids and its solution for tight naturally fractured sandstone reservoirs. *Geofluids.* **2017**, *2017*, 1−9.

(13) Zhang, L. F.; Z Zhou, F. J.; Zhang, S. C.; Li, Z.; Wang, J.; Wang, Y. C. Evaluation of permeability damage caused by drilling and fracturing fluids in tight low permeability sandstone reservoirs. *J. Pet. Sci. Eng.* **2019**, *175*, 1122−1135.

(14) Zhang, L. F.; Zhou, F. J.; Mou, J. Y.; Xu, G. Q.; Zhang, S. C.; Li, Z. A new method to improve long-term fracture conductivity in acid fracturing under high closure stress. *J. Pet. Sci. Eng.* **2018**, *171*, 760−770.

(15) Yang, Y. F.; Li, Y. W.; Yao, J.; Zhang, K.; Iglauer, S.; Luquot, L.; Wang, Z. B. Formation damage evaluation of a sandstone reservoir via pore-scale X-ray computed tomography analysis. *J. Pet. Sci. Eng.* **2019**, *183*, No. 106356.

(16) Guo, J. C.; Yang, L. I.; Wang, S. B. Adsorption damage and control measures of slick-water fracturing fluid in shale reservoirs. *Petrol Explor Dev.* **2018**, *45*, 336−342.

(17) Zhang, L. F.; Zhou, F. J.; Zhang, S. C.; Wang, Y. C.; Wang, J.; Wang, J. Investigation of water-sensitivity damage for tight low-permeability sandstone reservoirs. *ACS omega.* **2019**, *4*, 11197−11204.

(18) Huang, K.; Yang, F. Physical property analysis and sensitivity damage evaluation of tight sandstone gas reservoirs. *Int. J. Energy.* **2023**, *2*, 84−87.

(19) Li, H.; Liu, Z. L.; Jia, N. H.; Cheng, X.; Yang, J.; Cao, L. L.; Li, B. A new experimental approach for hydraulic fracturing fluid damage of ultradeep tight gas formation. *Geofluids.* **2021**, *2021*, 1−9.

(20) Li, Y. Z.; Jiang, G. C.; Li, X. Q.; Yang, L. L. Quantitative investigation of water sensitivity and water locking damages on a low-permeability reservoir using the core flooding experiment and NMR test. *ACS omega.* **2022**, *7*, 4444−4456.

(21) Yang, Y. F.; Li, Y. W.; Yao, J.; Zhang, K.; Iglauer, S.; Luquot, L.; Wang, Z. B. Formation damage evaluation of a sandstone reservoir via pore-scale X-ray computed tomography analysis. *J. Pet. Sci. Eng.* **2019**, *183*, No. 106356.

(22) Jia, H.; Huang, P.; Wang, Q. X.; Han, Y. G.; Wang, S. Y.; Zhang, F.; Pan, W.; Lv, K. H. Investigation of inhibition mechanism of three deep eutectic solvents as potential shale inhibitors in water-based drilling fluids. *Fuel.* **2019**, *244*, 403−411.

(23) Xu, D. Q.; Chen, S. H.; Chen, J. F.; Xue, J. S.; Yang, H. Study on the imbibition damage mechanisms of fracturing fluid for the whole fracturing process in a tight sandstone gas reservoir. *Energies.* **2022**, *15*, 4463.

(24) Zhang, H.; Zhong, Y.; Kuru, E.; Kuang, J. C.; She, J. P. Impacts of permeability stress sensitivity and aqueous phase trapping on the tight sandstone gas well productivity-A case study of the Daniudi gas field. *J. Pet. Sci. Eng.* **2019**, *177*, 261−269.
(25) Bahrami, H.; Rezaee, R.; Clennell, B. Water blocking damage in hydraulically fractured tight sand gas reservoirs: An example from Perth Basin, Western Australia. *J. Pet. Sci. Eng.* **2012**, *88*, 100−106.
(26) Helland, J. O.; Jettestuen, E. Mechanisms for trapping and mobilization of residual fluids during capillary-dominated three-phase flow in porous rock. *Water Resour. Res.* **2016**, *52*, 5376−5392.
(27) Rostami, A.; Nguyen, D. T.; Nasr-El-Din, H. A. Laboratory studies on fluid-recovery enhancement and mitigation of phase trapping by use of microemulsion in gas sandstone formations. *Spe Prod. Oper.* **2016**, *31*, 120−132.
(28) Wu, Y. J.; Dong, X. Y.; Zheng, X. S.; Lu, X. H.; Li, D.; Pan, M.; Zeng, W. Q.; He, J. X. Study on water lock releasing agent for gas reservoir in Sulige TaoX block. *Chemical Engineering of Oil & Gas.* **2022**, *51*, 89−94.
(29) Xu, Y.; Tang, Y. F.; Li, W.; Liu, Y. Q.; Jing, X. W. Rearch on a new type of cleanup additive based on degradable gemini fluorocarbon surfactant. *Chemical Engineering of Oil & Gas.* **2019**, *48*, 62−65.
(30) Tang, H. M.; Tang, H. X.; He, J.; Zhao, F.; Zhang, L. H.; Liao, J. J.; Wang, Q.; Yuan, X. F. Damage mechanism of water-based fracturing fluid to tight sandstone gas reservoirs: Improvement of The Evaluation Measurement for Properties of Water-based Fracturing Fluid: SY/T 5107−2016. *Natural Gas Industry B* **2021**, *8*, 163−172.
(31) Groen, J. C.; Peffer, L. A. A.; Pérez-Ramírez, J. P. Pore size determination in modified micro- and mesoporous materials. Pitfalls and limitations in gas adsorption data analysis. *Micropor Mesopor Mater.* **2003**, *60*, 1−17.
(32) Pfeifer, P.; Avnir, D. Chemistry in noninteger dimensions between two and three. I. Fractal theory of heterogeneous surfaces. *J. Chem. Phys.* **1983**, *79*, 3558−3565.
(33) Naitonal Energy Administration; *Recommended practice for evaluation of water sensitivity of shale: NB/T 14022−2017*. Petroleum Industry Press: Beijing, 2017.
(34) Zhong, Y.; Zhang, H.; Kuru, E.; Kuang, J. C.; She, J. P. Mechanisms of how surfactants mitigate formation damage due to aqueous phase trapping in tight gas sandstone formations. *Colloids Surf., A* **2019**, *573*, 179−187.
(35) Huang, H.; Babadagli, T.; Chen, X.; Li, H. Z.; Zhang, Y. M. Performance comparison of novel chemical agents for mitigating water-blocking problem in tight gas sandstones. *SPE. Reser. Eval. Eng.* **2020**, *23*, 1150−1158.

https://doi.org/10.1021/acsomega.3c05461
ACS Omega 2023, 8, 37461−37470